

Combined First and Second Order Variational Approaches for Image Processing

Gabriele Steidl*

February 24, 2015

Abstract

Variational methods in imaging are nowadays developing towards a quite universal and flexible tool, allowing for highly successful approaches on tasks like image restoration, registration, segmentation, super-resolution, and estimation of flow fields. We review recent progress in mathematical image processing by combining first and second order derivatives in the regularization term of variational models. We demonstrate the power of the proposed methods by two rather different applications. The approaches make use of two different splitting methods of the functional to obtain iterative numerical schemes which require in each step only the computation of simple proximal mappings.

MSC Classification: 49J40, 49M29, 49M37, 49N45, 52A41,65K10

Keywords: Mathematical image analysis, variational models, primal-dual algorithms, higher order models, optical flow, strain tensor, cyclic proximal point algorithm, cyclic data

1 Introduction

Mathematical image processing is an innovative, rapidly developing branch of applied mathematics which involves various mathematical fields as applied harmonic analysis, inverse problems, numerical analysis, partial differential equations, mathematical morphology, probabilistic and statistical methodologies, and variational methods. In this paper we focus on the later one. More precisely, we will consider non-smooth, convex functionals with generalized total variation regularization terms which include second order derivatives. Let us first have a look at the objects we are dealing with.

*University of Kaiserslautern, Dept. of Mathematics, Paul Ehrlich Str. 31, Germany

1.1 Digital images

A digital two-dimensional gray-value image f can be considered as a mapping from a two-dimensional grid $\mathcal{G} := \{1, \dots, m\} \times \{1, \dots, n\}$ into a discrete subset $\{0, \dots, L - 1\}$ of \mathbb{N} , whose values can be visualized as gray values by a computer screen. Humans can distinguish between 64 gray values; however often 8-bit images with $L = 256$ different values are considered. When dealing with images we usually assume that f maps into the real numbers (or an interval) instead of $\{0, \dots, L - 1\}$ and apply a subsequent quantization (rounding). In Section 4 we present a typical discrete approach to a variational problem via finite differences which relies on this image model.

From the analytical point of view it is often more intuitive to consider gray-value images as mappings from a bounded domain $\Omega \subset \mathbb{R}^2$ into the real numbers. Then the functionals have to be minimized over certain (infinite dimensional) function spaces. (It is not clear to which function spaces natural images really belong, see [56].) For the numerical treatment one has finally to apply a discretization, but not necessary a finite difference approach. Here we refer to the books [38, 85] which focus on continuous models. In Sections 2 and 3 we start with a continuous variational approach which may be useful for people having some background in function spaces. It is possible to skip these sections and move directly to the discrete, finite dimensional setting on \mathcal{G} in Section 4.



Figure 1. Two frames of a traffic scene and optical flow estimation by a first order method similar to [24]. (Image source: <http://i21www.ira.uka.de/image-sequences/>).

Gray-value images are the „simplest” digital images. Often we have to deal with vector-valued functions $f : \mathcal{G} \rightarrow \mathbb{R}^d$. For two-dimensional flow fields appearing, e.g., in motion estimation we have $d = 2$. A typical example is shown in Fig. 1. Based on the estimation of optical flow fields we will estimate strain tensors in Section 5. For hyperspectral images d is rather large, e.g., $d = 256$. For color images on a computer screen we have usually $d = 3$ and the three components represent the colors red (R), green (G) and blue (B) (again each color is in $\{0, \dots, L - 1\}$, but for simplicity

we assume that we have real values). Depending on the visualization device other color spaces than RGB are used. One example is the HSV space which splits the image into its hue, saturation and value of brightness. The hue describes in each area of an image the dominant color ingredient that one really perceives. It is a cyclic value between 0 (for red) and 2π , see Fig. 2. While it is quite hard to determine a certain color by just addressing its RGB components, the HSV space is more intuitive to the human color reception system. Fig. 3 shows the decomposition of an image into its HSV components. In variational models with vector-valued images, the meaningful coupling of the different vector components is an interesting ongoing research topic, see [52, 81]. We cannot address this circumvent topic in the present paper.

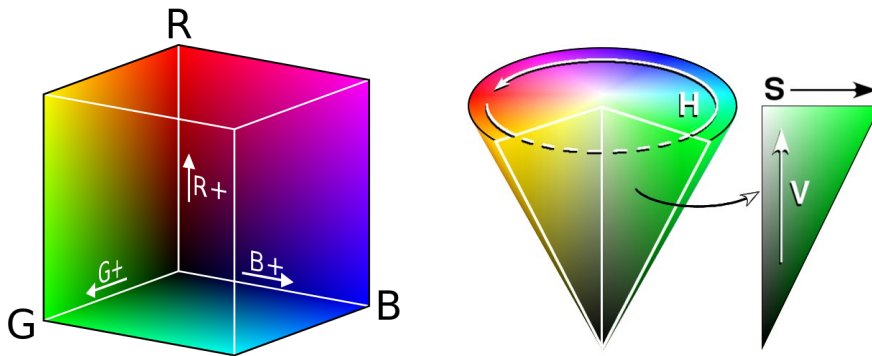


Figure 2. Color representation systems: RGB cube and HSV cone. (Image sources: <http://commons.wikimedia.org/Maklaan> and <http://commons.wikimedia.org/Fanghong>).

Finally, in various applications we have to replace \mathbb{R}^d by a d -fold Riemannian manifold \mathcal{M}^d . Typical examples are the manifold of symmetric positive definite matrices which appears in diffusion tensor MRI, the rotation group $SO(3)$ or the n -sphere \mathbb{S}^n . Often cyclic data have to be handled which is the topic of Section 6. An example of an \mathbb{S}^1 -valued image is the hue image in Fig. 3. Although the \mathbb{S}^1 is a rather simple manifold the new techniques from convex optimization recently used to minimize the variational functionals do not simply carry over to this setting.

1.2 Variational Models

In image restoration we are interested in finding an unknown image u_0 given its modified version f . Mathematically the corruption of the original image can be often described by the application of a linear operator K to u_0 . For example, for blurred images, K is a convolution operator, and for images with missing areas a masking operator, see Fig. 11. The restoration of missing pixels is called „inpainting”. In addition the result of the linear

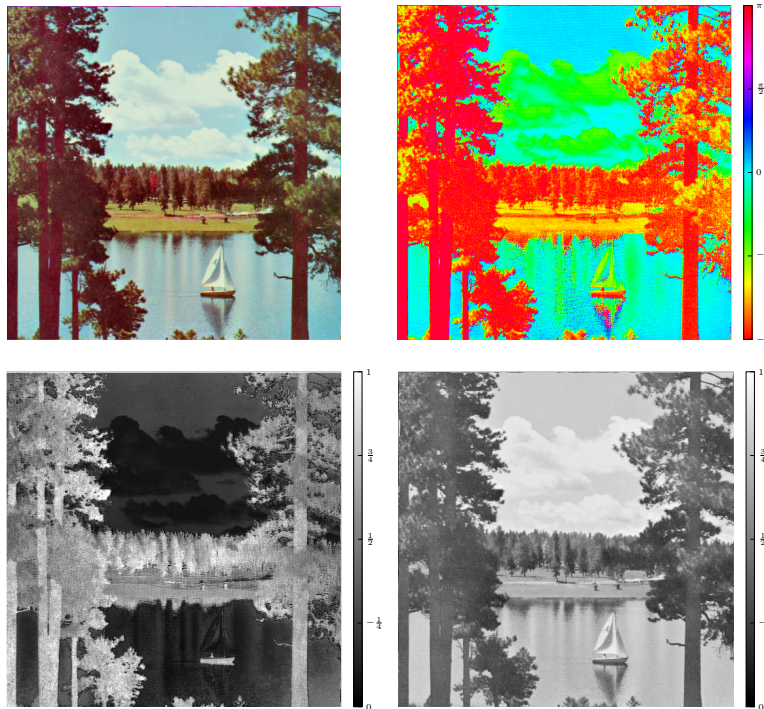


Figure 3. Top: Original image *sailboat* and its hue. Bottom: Its saturation and value of brightness. (Image source: USC-SIPI Image Database) .

transform Ku_0 is often corrupted by noise. Depending on the application we have to tackle with different kind of noise. In this paper we simply focus on additive white Gaussian noise. In summary, the observed image is

$$f = Ku_0 + \eta,$$

where η is the realization of a Gaussian independently identically distributed random vector with mean zero and variance σ . In pure denoising problems K is just the identity operator. Often K is known which is also assumed in this paper. If K is also unknown, the reconstruction problem becomes much harder. The deblurring problem with an unknown convolution kernel is called „blind deblurring”. The problem to reconstruct u_0 from $f \approx Ku_0$ is ill-posed or ill-conditioned, since the operator K is either not invertible as for the inpainting problem or has no continuous inverse (resp. is ill-conditioned in the finite dimensional setting) as in the deblurring problem such that small errors in f are amplified if we just apply the inverse operator to f . Problems of this kind were traditionally considered in the field of inverse problems, see [14, 44, 66]. A general approach is to minimize an appropriate

functional of the form

$$\mathcal{D}(Ku; f) + \alpha\mathcal{R}(u) \rightarrow \min_u, \quad (1)$$

and to take a minimizer as approximation of u_0 . The so-called data fidelity term \mathcal{D} measures the deviation of Ku from f . It is often smooth and convex and becomes minimal if $Ku = f$. The regularizing term \mathcal{R} is required to make the problem well-posed. Moreover, it contains a priori knowledge (desires) on the reconstructed images and is also called image prior. The design of appropriate regularizers such that the minimizers of (1) have certain properties like the preservation of important image structures while keeping the functional analytically and numerically feasible is a challenging task. Since such goals cannot be achieved with differentiable regularization terms, current practice almost exclusively uses non-smooth regularization functionals like the total variation (TV) [79] and generalizations thereof, or ℓ_1 -norms of coefficients arising from scalar products with frame systems, see, e.g., [48, 73]. The analysis of such functionals requires tools from functional analysis as well as convex analysis. Finally, the regularization parameter α balances the influence of the data and the regularization term. Its appropriate choice is very important and an ongoing topic of research. Several techniques were developed to address this task as Morozov's discrepancy principle [75], the L-curve criterion [68], the generalized cross-validation [98], normalized cumulative or residual periodogram approaches [80], and variational Bayes' approaches [4, 57]. For an overview over the first methods we refer to [58] and for recent relations between penalized and constrained problems to [95] and the references therein. In this paper we do not pay attention to an automatic adjustment of the parameters but tune them by hand according to some error measures.

1.3 Algorithms

The efficient solution of non-smooth variational problems of the form (1) demands for appropriate algorithms. Taking into account the specific structure of the functional as a sum of different convex terms, splitting algorithms are a quite canonical choice. Their strength consists in the splitting of the original problem into a sequence of smaller ones which are easy to compute.

Operator splitting methods were first applied to the numerical solution of partial differential equations in the 60th of the last century, e.g., by Douglas and Rachford 1956 [43]. Here the splitting was applied to linear, single-valued operators in order to solve a certain linear system of equations efficiently. More than 20 years later these splitting methods were generalized in the convex analysis community to the solution of inclusion problems, where the linear operators have to be replaced by nonlinear, set-valued, monotone operators. Here we refer to the initial paper of Lions and Mercier [71]

which was followed by many others. Again after more than 20 years these methods became popular in image processing starting with the work of Chambolle and Wajs [37]. Operator splittings in conjunction with (augmented) Lagrangian methods and primal-dual methods have recently received a lot of interest, for an overview see, e.g., [25, 36]. Interestingly, one of the first papers in imaging in this direction by Goldstein and Osher [53] proposes a so-called alternating split Bregman algorithm. Later it turned out that from one point of view this algorithm coincides with the Douglas-Rachford algorithm applied to the dual problem and from another point of view with the alternating direction method of multipliers based on the augmented Lagrangian, see [45, 86]. In this paper we will show how primal-dual methods can be applied to minimize appropriate functionals which were proposed in two recent applications, namely in the computation of local deformations in materials from a sequence of image frames via optical flow estimation [7], and the denoising of phase-valued images [10].

2 Continuous First Order Variational Models

Let $\Omega \subset \mathbb{R}^2$ be a bounded Lipschitz domain. Assume that $f \in L_2(\Omega)$ was obtained by applying a linear operator K , e.g., a convolution operator, to an unknown function $u_0 \in L_2(\Omega)$ and the result was corrupted by additive white Gaussian noise. Then the log likelihood approach leads to the minimization of the data fidelity term

$$\mathcal{D}(Ku; f) := \frac{1}{2} \|f - Ku\|_{L_2}^2. \quad (2)$$

For other noise statistics the data term must be replaced by appropriate ones as the Kullback-Leibler divergence in case of Poisson or certain kind of multiplicative noise, see, e.g., [82, 89] or the L_1 norm for impulse noise [26]. For the choice of the regularizer, the $W^{1,2}$ semi-norm $\mathcal{R}(u) := \|\nabla u\|_{L_2}^2$ has a long tradition:

$$\frac{1}{2} \|f - Ku\|_{L_2}^2 + \alpha \int_{\Omega} |\nabla u|^2 dx, \quad \alpha > 0.$$

However, this model is not appropriate for most image processing tasks, simply since the minimizer is too smooth: From the continuous point of view the minimizing image must be in the „smooth” Sobolev space $W^{1,2}$. In particular, for the identity operator K , the gradient flow of the corresponding Euler-Lagrange equation is the linear partial differential equation $u_t = \alpha \Delta u - u + f$. Hence the minimizer is a uniformly smoothed image which does not take prominent structures of f like edges into account. In summary, it is impossible to reconstruct sharp edges with semi-norms of $W^{1,p}$, $p > 1$. This is demonstrated in Fig. 4.

This drawback leads to the consideration of new classes of non-smooth regularizers, where the TV regularization [79] is certainly the most frequently applied one in variational image processing. Let $\text{BV}(\Omega)$ denote the space of functions of bounded variation, i.e., the Banach space of functions $u : \Omega \rightarrow \mathbb{R}$ with finite norm $\|u\|_{\text{BV}} := \|u\|_{L_1} + \text{TV}(u)$, where

$$\text{TV}(u) := \sup \left\{ \int_{\Omega} u \operatorname{div} \varphi \, dx : \varphi \in C_c^1(\Omega, \mathbb{R}^2), \|\varphi\|_{\infty} \leq 1 \right\},$$

and $\|\varphi\|_{\infty} := \|(\varphi_1^2 + \varphi_2^2)^{\frac{1}{2}}\|_{L_{\infty}}$. Here $C_c^1(\Omega, \mathbb{R}^2)$ denotes the space of continuously differentiable vector-valued functions on Ω with compact support. The distributional first order derivative Du of u is a vector-valued Radon measure with total variation $|Du|(\Omega) = \text{TV}(u)$. In particular, for $u \in W^{1,1}(\Omega)$ the TV term reduces to $\text{TV}(u) = \int_{\Omega} |\nabla u| \, dx$ so that our functional becomes

$$\frac{1}{2} \|f - Ku\|_{L_2}^2 + \alpha \int_{\Omega} |\nabla u| \, dx, \quad \alpha > 0.$$

Since the gradient of a constant area is zero, the functional does not penalize constant areas which leads to well-known staircasing effect. A good overview on total variation for image analysis in particular the relation between the TV functional and the perimeter of level sets can be found in [27]. A typical example can be seen in Fig. 4. We mention that smoothed versions of the absolute value function like its Moreau envelope also known as Huber function $\psi := \min_t \frac{1}{2\varepsilon}(\cdot - t)^2 + |\cdot|$ or $\psi := \sqrt{|\cdot|^2 + \varepsilon^2}$ can reduce the staircasing artifact to some extent but have other drawbacks.

3 Continuous Second Order Variational Models

A successful method to cope with the staircasing effect is to incorporate higher order derivatives into the regularization term, in particular second order derivatives. For simplicity we incorporate the regularization parameters within the regularizer \mathcal{R} in the rest of the paper.

Let $\text{BV}(\Omega, \mathbb{R}^2)$ denote the space of vector-valued functions $u = (u_1, u_2)$ of bounded variation, where the above definition of TV has to be modified by $\int_{\Omega} u_1 \operatorname{div} \varphi_1 + u_2 \operatorname{div} \varphi_2 \, dx$. We consider the space of bounded Hessians $\text{BH}(\Omega) := \{u \in W^{1,1}(\Omega) : \nabla u \in \text{BV}(\Omega, \mathbb{R}^2)\}$ with norm $\|u\|_{\text{BH}} = \|u\|_{\text{BV}} + |D^2u|(\Omega)$ and $|D^2u| = |D(\nabla u)|$, see [2, 40]. There are three established ways for combining first and second order derivatives in the regularization term:

- i) The first approach minimizes the functional (1) with data term (2) and regularization term

$$\mathcal{R}(u) := \int_{\Omega} \alpha |\nabla u| \, dx + \beta |D^2u|(\Omega)$$

over $\text{BV}(\Omega, \mathbb{R}^2)$. For applications in imaging we refer to [76].

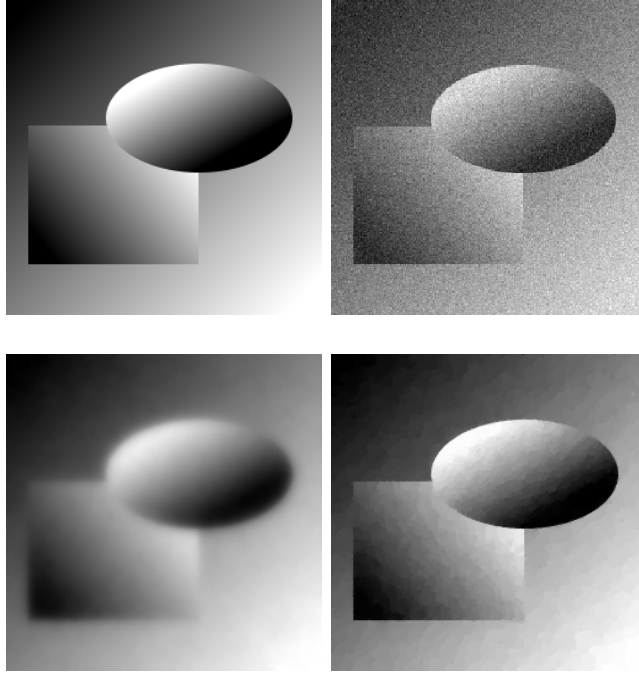


Figure 4. Top: Original image and noisy image. Bottom: restored images with $W^{1,2}$ regularization and with TV regularization. The $W^{1,2}$ regularized method produces a smoothed images where important image structures get lost. The TV regularized approach keeps sharp edges, but introduces a staircasing effect in non flat areas. (Image from [41]).

- ii) The second method makes use of the infimal convolution of two (extended) functionals \mathcal{R}_i , $i = 1, 2$ which is defined by

$$(\mathcal{R}_1 \square \mathcal{R}_2)(u) := \inf_{v+w=u} \mathcal{R}_1(v) + \mathcal{R}_2(w).$$

The infimal convolution is the counterpart of the 'usual' convolution of functions in the max-plus algebra. More precisely, the regularization term consists of the infimal convolution of $\mathcal{R}_1(v) := \text{TV}(v)$ and $\mathcal{R}_2(w) := |D^2 w|$ for u (and v) in $\text{BV}(\Omega)$ and $w \in W^{1,1}$ with $\nabla w \in \text{BV}(\Omega, \mathbb{R}^2)$:

$$\mathcal{R}(u) := \inf_{v+w=u} \alpha \text{TV}(v) + \beta |D^2 w|(\Omega).$$

For $\nabla v \in W^{1,1}(\Omega, \mathbb{R}^2)$ and $u \in W^{1,1}(\Omega)$ the whole functional can be rewritten as

$$\frac{1}{2} \|f - Ku\|_{L^2}^2 + \int_{\Omega} \alpha |\nabla u - \nabla w| dx + \beta |\nabla^2 w| dx \rightarrow \min_{u,w} \quad (3)$$

Roughly speaking, for $K = Id$, we 'first' approximate locally the gradient of the function f by ∇w that has itself a low total variation and then find u as an approximation of f such that $u - w$ has a low total variation. As a consequence we do not get anymore an almost piecewise constant minimizer. This regularization method was introduced in imaging by Chambolle and Lions [28]. For a recent generalization called ICTV we refer to [63].

- iii) A conceptually different approach was recently proposed by Bredies, Kunisch and Pock [21]; for the discrete setting see also [87]. Here the regularization term is the so-called total generalized variation (TGV^2) defined by

$$\begin{aligned} \mathcal{R}(u) &= TGV_{(\alpha,\beta)}^2(u) \\ &:= \sup \left\{ \int_{\Omega} u \operatorname{div}^2 \varphi \, dx : \varphi \in C_c^2(\Omega, \operatorname{Sym}(\mathbb{R}^2)), \|\varphi\|_{\infty} \leq \alpha, \|\operatorname{div} \varphi\|_{\infty} \leq \beta \right\} \end{aligned}$$

where $C_c^2(\Omega, \operatorname{Sym}(\mathbb{R}^2))$ denotes the space of two times continuously differentiable 2-tensor fields with compact support in Ω and $\operatorname{div}^k \varphi := \operatorname{tr}(\nabla^k \otimes \varphi)$, $k = 1, 2$. In other words, we have for $\varphi = (\varphi_{1,1}, \varphi_{1,2}, \varphi_{2,2})$ that

$$\operatorname{div}^2 \varphi = \partial_{xx} \varphi_{1,1} + (\partial_{xy} + \partial_{yx}) \varphi_{1,2} + \partial_{yy} \varphi_{2,2}$$

and

$$\operatorname{div} \varphi(e_1) = \partial_x \varphi_{1,1} + \partial_y \varphi_{1,2}, \quad \operatorname{div} \varphi(e_2) = \partial_x \varphi_{1,2} + \partial_y \varphi_{2,2}.$$

An alternative definition of $TGV_{(\alpha,\beta)}^2$ is given by

$$TGV_{(\alpha,\beta)}^2(u) := \min_{y \in \operatorname{BD}(\Omega)} \alpha |Du - y|(\Omega) + \beta |\mathcal{E}y|(\Omega),$$

where $\operatorname{BD}(\Omega)$ is the space of functions of bounded deformation and $\mathcal{E}y$ is the distributional symmetrised gradient of y , see [22]. In a simplified version, instead of (3) we get

$$\frac{1}{2} \|f - Ku\|_{L_2}^2 + \int_{\Omega} \alpha |\nabla u - y| \, dx + \beta |\nabla y| \, dx \rightarrow \min_{u,y}$$

There are several other approaches which make use of higher order derivatives including weighted versions of the Laplacian [33, 74], bounded Hessians (without first order terms) [13, 31, 60, 62, 72, 84], and Euler's elastica [32, 93]. In [69] the spectral norm of the discrete Hessian is used as a regularizer. The relation to higher order diffusion filters was analyzed by Didas et al. in [42]. For discrete versions of the above approaches we refer to [87, 88].

4 Discrete Second Order Variational Models

For computations we need a discrete version of the functionals in the previous section. We consider gray-value images as functions $f: \mathcal{G} \rightarrow \mathbb{R}$ defined on a rectangular grid $\mathcal{G} := \{1, \dots, m\} \times \{1, \dots, n\}$ and make use of finite difference approximations for the differential operators. Indeed the appropriate discretization plays an important role in certain imaging applications, see, e.g., [100, 102]. In particular, if the second order derivatives come into the play and the identities satisfied by the continuous operators should be preserved it becomes necessary to work on more than one grid. One possibility is the use of the finite mimetic difference method, see, e.g., [65, 103, 104].

In the following we will use simple forward difference operators. To have a convenient vector-matrix notion it is usual to reorder f columnwise into a vector $\text{vec } f$ of length $N := mn$. If the meaning is clear from the context we keep the notation f instead of $\text{vec } f$.

The discretization of the data term (2) with a linear operator K follows just by considering the functions on the grid and taking the Euclidean norm of their reshaped form:

$$\mathcal{D}(Ku; f) := \frac{1}{2} \|f - Ku\|_2^2, \quad K \in \mathbb{R}^{N,N}.$$

For discretizing the regularization term, let

$$D_n := \begin{pmatrix} -1 & 1 & & & \\ & & \ddots & \ddots & \\ & & & -1 & 1 \\ & & & & 0 \end{pmatrix} \in \mathbb{R}^{n,n}$$

be the discrete forward difference operator with respect to mirror (Neumann) boundary conditions and

$$\nabla := \begin{pmatrix} D_x \\ D_y \end{pmatrix} \quad \text{with} \quad D_x := I_n \otimes D_m, \quad D_y := D_n \otimes I_m$$

be the discrete gradient operator. Here \otimes denotes the Kronecker product operator. Further, let

$$\nabla^2 := \begin{pmatrix} D_{xx} \\ D_{xy} + D_{yx} \\ D_{yy} \end{pmatrix}, \quad \tilde{\nabla} := \begin{pmatrix} D_x^T & 0 \\ D_y^T & D_x^T \\ 0 & D_y^T \end{pmatrix}$$

be a second order difference operator and the symmetrised discrete gradient operator of a vector field, resp., where

$$\begin{aligned} D_{xx} &:= -I_n \otimes D_m^T D_m, & D_{yy} &:= -D_n^T D_n \otimes I_m, \\ D_{xy} &:= -D_n^T \otimes D_m, & D_{yx} &:= -D_n \otimes D_m^T. \end{aligned}$$

Then the regularization terms in i) - iii) become

$$\text{i) } \mathcal{R}(u) = \alpha \|\nabla u\|_{2,1} + \beta \|\nabla^2 u\|_{2,1},$$

$$\text{ii) } \mathcal{R}(u) = \min_{w \in \mathbb{R}^N} \alpha \|\nabla(u - w)\|_{2,1} + \beta \|\nabla^2 w\|_{2,1},$$

$$\text{iii) } \mathcal{R}(u) = \min_{y \in \mathbb{R}^{2N}} \alpha \|\nabla u - y\|_{2,1} + \beta \|\tilde{\nabla} y\|_{2,1},$$

where we use the mixed $L_2(\mathbb{R}^d) - L_1(\mathbb{R}^N)$ norms defined for $x \in \mathbb{R}^{Nd}$ as

$$\|x\|_{L_2(\mathbb{R}^d), L_1(\mathbb{R}^N)} = \|x\|_{2,1} := \sum_{i=1}^N \left(\sum_{j=0}^{d-1} x_{jN+i}^2 \right)^{\frac{1}{2}},$$

see [87, 88] for the functionals ii) and iii). Fig. 5 shows the denoising results for the image in Fig. 4 top, right.

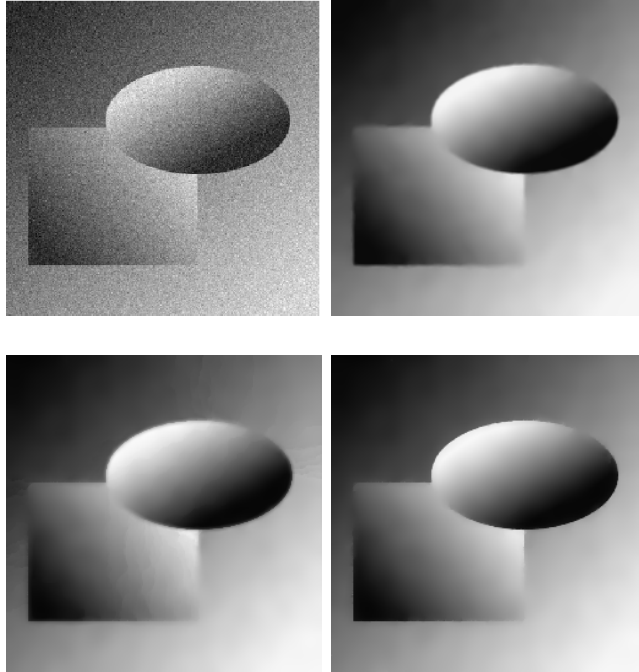


Figure 5. Top: Noisy image from Fig. 4 and denoised images with regularization i). Bottom: Denoised images with regularization ii), and iii).

There are numerous applications of second order models in image processing. In the following we present two recent ones, namely, the computation of local deformations in materials from a sequence of image frames via optical flow estimation [7], and the denoising of phase-valued images [10].

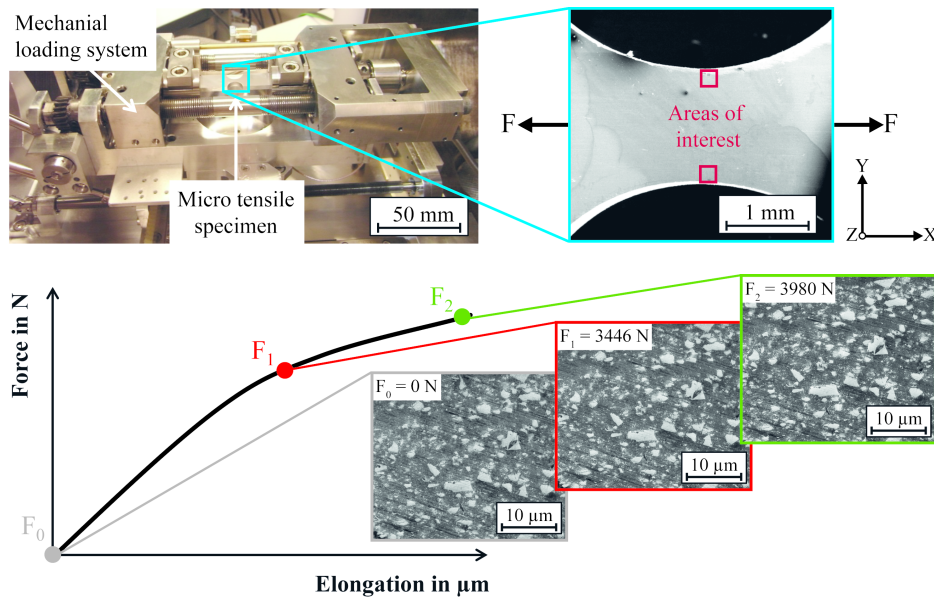


Figure 6. Experimental setup for the tensile test inside a scanning electron microscope. Load-deformation diagram with three selected micrographs (1024×884 pixel; size $51\mu\text{m} \times 44\mu\text{m}$) taken under increasing load. (Image credit: S. Schuff, Department of Mechanical and Process Engineering, University of Kaiserslautern.)

The first application is interesting since the the strain is directly computed within the numerical algorithm by an appropriate variable splitting. The second application establishes for the first time a second order model for cyclic data.

5 Computation of Local Deformation for Multi-phase Metallic Materials

5.1 Motivation

The (Cauchy) strain tensor plays a fundamental role in mechanical engineering for deriving local mechanical properties of materials. In this subsection we calculate local strains of silicon carbide particle reinforced aluminum matrix composites from a sequence of scanning electron microscope images acquired during tensile tests, where the micro-specimen is pulled in horizontal direction and elongates with increasing force. Fig. 6 illustrates the experimental setup and the resulting image sequence schematically*. For de-

*The scanning electron microscope tensile tests were performed at the Department of Mechanical and Process Engineering, University of Kaiserslautern by Dr. F. Balle, Prof. Dr. D. Eifler, and S. Schuff).

formations of a continuum body the strain tensor is defined via the gradient of the displacement $u = (u_1, u_2)$, i.e.,

$$\varepsilon = \begin{pmatrix} \varepsilon_{xx} & \varepsilon_{xy} \\ \varepsilon_{yx} & \varepsilon_{yy} \end{pmatrix} := \frac{1}{2}(\nabla u^\top + \nabla u) = \begin{pmatrix} \partial_x u_1 & \frac{1}{2}(\partial_y u_1 + \partial_x u_2) \\ \frac{1}{2}(\partial_y u_1 + \partial_x u_2) & \partial_y u_2 \end{pmatrix}.$$

We will especially focus on ε_{xx} which describes the change in displacement u_1 for the horizontal direction. A positive value indicates tension and a negative one compression.

One of the few papers which addresses the (Lagrangian) strain tensor computation by a variational method is [59] by Hewer et al.. The authors propose a smooth fourth order optical flow model which directly computes the strain tensor from an image sequence obtained in a biaxial tensile test with an elastomer. In contrast to our paper they were interested in the macro scale behavior and compute the minimizer of their smooth energy function by solving the corresponding Euler-Lagrange equations. For engineering purposes there are some approaches and commercial software packages based on image correlation such as [19, 83, 94, 99]. However, these methods are only suitable for computing the strain on a macro scale. Variational methods for optical flow estimation go back to [64]. There is a vast number of refinements and extensions of their approach and we refer to [9, 61] for a comprehensive overview. In particular higher order optical flow models were successfully used, e.g., in [1, 96, 103, 104, 105].

5.2 Variational Model

As for images we consider flow fields $u = (u_1, u_2): \mathcal{G} \rightarrow \mathbb{R}^2$ on a rectangular grid and use the reordering $\text{vec } u = ((\text{vec } u_1)^\top, \text{vec } u_2)^\top \in \mathbb{R}^{2N}$. As usual we identify u with $\text{vec } u$ if the meaning is clear from the context.

In the task at hand we focus on two images f_1 and f_2 from the tensile test belonging to different tensions. For multiframe treatments in optical flow we refer, e.g., to [99]. The **data term** in (1) relies on an invariance requirement between these images. Here we focus on the brightness invariance assumption which reads in the continuous setting as

$$f_1(x, y) - f_2((x, y) - u(x, y)) \approx 0, \quad u = (u_1, u_2). \quad (4)$$

Using a first order Taylor expansion around an initial optical flow field $\bar{u} = (\bar{u}_1, \bar{u}_2)$ gives

$$f_2((x, y) - u) \approx f_2((x, y) - \bar{u}) - \begin{pmatrix} \partial_x f_2 \\ \partial_y f_2 \end{pmatrix} ((x, y) - \bar{u}) \cdot (u(x, y) - \bar{u}(x, y)). \quad (5)$$

Later we will apply a coarse-to-fine scheme [3, 23] and use the result from one scale as an initialization for the next scale. By (5) the requirement (4) becomes

$$0 \approx f_1(x, y) - f_2((x, y) - \bar{u}) + \begin{pmatrix} \partial_x f_2 \\ \partial_y f_2 \end{pmatrix} ((x, y) - \bar{u}) \cdot (u(x, y) - \bar{u}(x, y)).$$

Note that $f_2((x, y) - \bar{u})$ is only well defined in the discrete setting, if $(i, j) - \bar{u}$ is in \mathcal{G} . Here, bilinear interpolation is used to compute values between grid points. Using a non-negative increasing function $\varphi: \mathbb{R} \rightarrow \mathbb{R}_{\geq 0}$ and considering only grid points $(x, y) = (i, j) \in \mathcal{G}$, the data term becomes

$$\sum_{(i,j) \in \mathcal{G}} \varphi \left(\begin{pmatrix} D_m f_2((i, j) - \bar{u}) \\ f_2((i, j) - \bar{u}) D_n^T \end{pmatrix} \cdot (u(i, j) - \bar{u}(i, j)) - f_2((i, j) - \bar{u}) + f_1(i, j) \right)$$

and for $\varphi(t) := |t|$ finally

$$\mathcal{D}(Ku; c) := \frac{1}{2} \|Ku + c\|_1, \quad K := (AB). \quad (6)$$

where $\|\cdot\|_1$ denotes the $L_1(\mathbb{R}^{2N})$ norm and

$$A := \text{diag} \left(\text{vec} \left(D_m f_2((i, j) - \bar{u}) \right) \right), \quad B := \text{diag} \left(\text{vec} \left(f_2((i, j) - \bar{u}) D_n^T \right) \right), \\ c := -\text{vec} \left(\begin{pmatrix} D_m f_2((i, j) - \bar{u}) \\ f_2((i, j) - \bar{u}) D_n^T \end{pmatrix} \cdot \bar{u}(i, j) - f_2((i, j) - \bar{u}) + f_1(i, j) \right).$$

For the choice of the **regularization term** we notice that the global displacement during insitu tensile testing can be roughly approximated by a plane. Therefore it makes sense to separate this global displacement from the local one using an infimal convolution regularization ii) (or the TGV² model which provides nearly the same results):

$$\mathcal{R}(u) = \inf_{v+w=u} \{ \alpha \|\nabla v\|_{2,1} + \beta \|\nabla^2 w\|_{2,1} \}, \quad (7)$$

where $\nabla u := (I_2 \otimes \nabla)u$ and $\nabla^2 u := (I_2 \otimes \nabla^2)u$.

It can be shown that in the case $\ker \begin{pmatrix} A & B \end{pmatrix} \cap \ker(\nabla) = \{\mathbf{0}\}$ there exists a minimizer of $J(u) := \mathcal{D}(Ku; c) + \mathcal{R}(u)$, see [7].

5.3 Algorithm

To solve the convex, non-smooth optimization problem (1) with data term (6) and regularization term (7) we apply a primal dual algorithm with an appropriate splitting. To this end, we rewrite the problem as

$$\min_{u,w,s,t} \{ \|Ku + c\|_1 + \alpha \|s\|_{2,1} + \beta \|t\|_{2,1} \} \quad (8)$$

$$\text{such that} \quad \begin{pmatrix} \nabla & -\nabla \\ 0 & \nabla^2 \end{pmatrix} \begin{pmatrix} u \\ w \end{pmatrix} = \begin{pmatrix} s \\ t \end{pmatrix}.$$

Indeed, we are not interested in u , but in its non-smooth part $v = u - w$ or more precisely in the strain $s = \varepsilon(v) = \nabla(u - w)$ which fortunately directly appears in the constraint.

With $F(u, w) := \|Ku + c\|_1$ and $G(s, t) := \alpha\|s\|_{2,1} + \beta\|t\|_{2,1}$ the Lagrangian of (8) reads

$$L((u, w, s, t), (p, q)) := F(u, w) + G(s, t) + \langle \nabla(u - w) - s, p \rangle + \langle \nabla^2 w - t, q \rangle$$

with the dual variable (p, q) . Then the primal problem (8) and its dual can be written as

$$(P) \min_{u, w, s, t} \max_{p, q} L((u, w, s, t), (p, q)), \quad (D) \max_{p, q} \min_{u, w, s, t} L((u, w, s, t), (p, q)).$$

Using the Fenchel dual of G defined by

$$G^*(p, q) := \max_{s, t} \left\langle \begin{pmatrix} s \\ t \end{pmatrix}, \begin{pmatrix} p \\ q \end{pmatrix} \right\rangle - G(s, t)$$

the problems become

$$(P) \min_{u, w} \max_{p, q} \{F(u, w) - G^*(p, q) + \langle \nabla(u - w), p \rangle + \langle \nabla^2 w, q \rangle\},$$

$$(D) \max_{p, q} \min_{u, w} \{F(u, w) - G^*(p, q) + \langle \nabla(u - w), p \rangle + \langle \nabla^2 w, q \rangle\}.$$

The Arrow-Hurwitz method consists in alternating the minimization over the primal and dual variables and adding a stabilizing quadratic terms:

$$\begin{aligned} \begin{pmatrix} u^{(r+1)} \\ w^{(r+1)} \end{pmatrix} &= \arg \min_{u, w} \left\{ F(u, w) + \left\langle \begin{pmatrix} \nabla(u - w) \\ \nabla^2 w \end{pmatrix}, \begin{pmatrix} p^{(r)} \\ q^{(r)} \end{pmatrix} \right\rangle + \frac{1}{2\tau} \left\| \begin{pmatrix} u \\ w \end{pmatrix} - \begin{pmatrix} u^{(r)} \\ w^{(r)} \end{pmatrix} \right\|_2^2 \right\}, \\ &= \text{prox}_{\tau F} \left(\begin{pmatrix} u^{(r)} \\ w^{(r)} \end{pmatrix} - \tau \begin{pmatrix} \nabla^T p^{(r)} \\ -\nabla^T p^{(r)} + (\nabla^2)^T q^{(r)} \end{pmatrix} \right) \\ \begin{pmatrix} p^{(r+1)} \\ q^{(r+1)} \end{pmatrix} &= \arg \min_{p, q} \left\{ G^*(p, q) - \left\langle \begin{pmatrix} \nabla(u^{(r+1)} - w^{(r+1)}) \\ (\nabla^2)w^{(r+1)} \end{pmatrix}, \begin{pmatrix} p \\ q \end{pmatrix} \right\rangle + \frac{1}{2\sigma} \left\| \begin{pmatrix} p \\ q \end{pmatrix} - \begin{pmatrix} p^{(r)} \\ q^{(r)} \end{pmatrix} \right\|_2^2 \right\} \\ &= \text{prox}_{\sigma G^*} \left(\begin{pmatrix} p^{(r)} \\ q^{(r)} \end{pmatrix} + \sigma \begin{pmatrix} \nabla(u^{(r+1)} - w^{(r+1)}) \\ (\nabla^2)w^{(r+1)} \end{pmatrix} \right), \end{aligned}$$

where the proximal mapping of a proper, closed convex function $g : \mathbb{R}^d \rightarrow \mathbb{R}^d \cup \{+\infty\}$ is defined by

$$\text{prox}_{\lambda g}(x) := \arg \min_y \frac{1}{2} \|x - y\|_2^2 + \lambda g(y), \quad \lambda > 0. \quad (9)$$

The internal parameters τ and σ of the algorithm can be found as in [54]. The basic idea behind this algorithm is that the proximal mappings can be simply computed (often there exists an analytical formula) for many functions used in variational image reconstruction models including the present ones.

Further, we apply an extrapolation step for the dual variable. This results in the primal-dual algorithm [29, 77] which is known as Chambolle-Pock algorithm in image processing. It was meanwhile generalized for various other functionals, e.g., in [20, 35, 97]. To cope with large displacements our algorithm was moreover updated by a coarse-to-fine scheme, see, e.g., [3, 23].

5.4 Numerical Results

In this tutorial we demonstrate the potential of our variational approach only by one example. We have applied our method to two different images f_2 obtained during the tensile test at a low ($F_1 = 3446N$) and a high ($F_2 = 3980N$) load level, see Fig. 6. Fig. 7 shows magnified micrographs (100×100 pixels, size $5\mu m \times 5\mu m$) of two different regions of the whole image where cracks were initiated. In both experiments the areas of computed high local strains correspond to crack areas in the material. It is remarkable that even under low load, when the cracks are not or hardly visible in the images, the strain tensor in the corresponding regions is high and seems to be a sensitive and useful tool to study crack initiation mechanisms of silicon carbide reinforced aluminum matrix composites. For details on the parameter choice see [7].

6 Restoration of Cyclic Data

6.1 Motivation

In various applications in image processing and computer vision the functions of interest take values on the circle \mathbb{S}^1 or on manifolds. In this subsection we deal with \mathbb{S}^1 -valued data which appear, e.g., in interferometric synthetic aperture radar [17, 18, 39], electroencephalogram data analysis [90], ground based astronomy [8, 30, 34, 55], circular statistics [47, 67] and color image restoration in HSV spaces. Handling phase-valued data with techniques for real-valued data introduces artifacts since the cyclic nature of the data is neglected. Fig. 1 shows a denoising example, where the so-called hue of an image which is phase-valued was denoised by minimizing the functional with squared L_2 data term and second order regularizer i) described in Sec. 4. Without taking the cyclic structure of the data into account the color values became completely wrong.

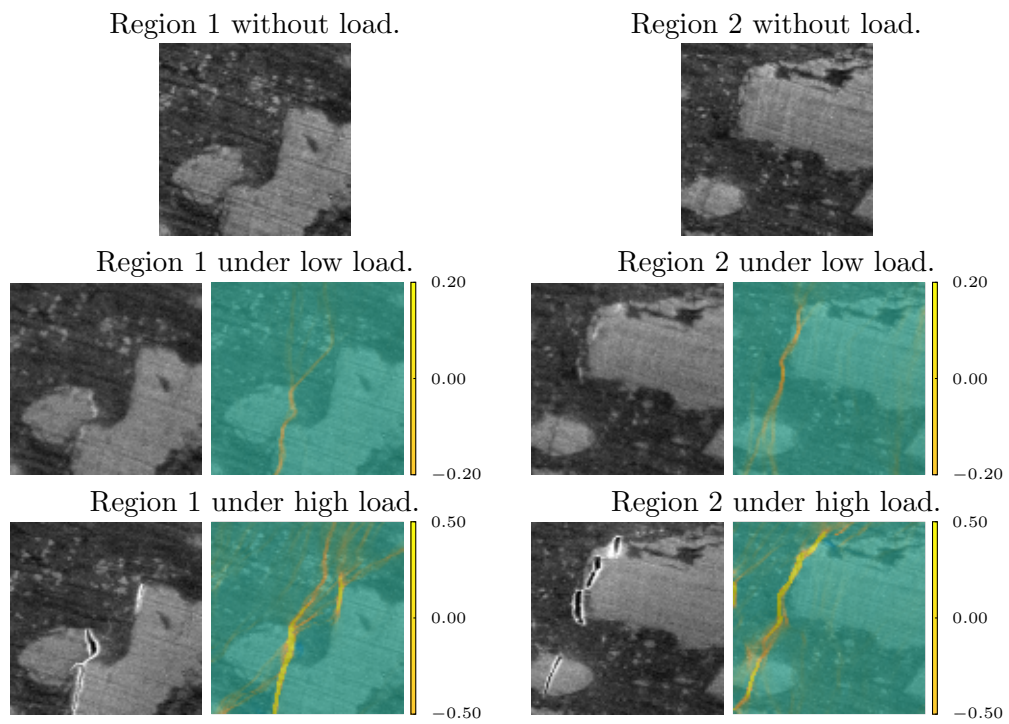


Figure 7. Results corresponding to images under low and high load. Zooms into two different regions. Top: The two initial image regions without load. Bottom: $\varepsilon_{xx} = \partial_x v_1$ for the two different regions under low and high load together with the image frame. The cracks in the high load images correspond to areas of high strain ε_{xx} . The high strain areas can also be detected from the low load images, where the cracks in the images themselves are (nearly) not visible.

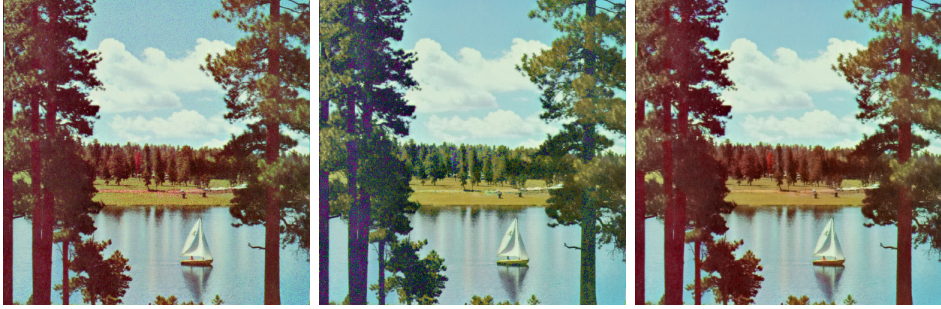


Figure 8. Left to right: Image *sailboat* from Fig. 3 with hue channel corrupted by wrapped Gaussian noise ($\sigma = 0.4$), denoised image by a second order method for real valued data (wrong colors are created), and by our method for cyclic data. Without taking the cyclic structure of the data into account we do not obtain correct colors.

Although the minimization of TV regularized functionals is among the most popular methods for edge-preserving image restoration such methods were only very recently applied to cyclic structures. The TV notation for functions with values on a manifold has been studied in [50, 51] using the theory of Cartesian currents. These papers were an extension of the previous work [49] where the authors focus on \mathbb{S}^1 -valued functions and show in particular the existence of minimizers of certain energies in $BV(\Omega)$. The first papers which apply a cyclic TV approach in imaging are [70, 91, 92]. In this subsection we want to incorporate second order differences into the energy functional for cyclic data. Indeed [10] is the first paper which uses higher order differences of cyclic data in regularization terms of energy functionals for image restoration.

6.2 Variational Model

We restrict our attention to functionals (1) with $K = Id$. First we replace the Euclidean distance by the geodesic distance $d_{\mathbb{S}^1}(p, q) := \arccos(\langle p, q \rangle)$ on $\mathbb{S}^1 := \{p_1^2 + p_2^2 = 1 : p = (p_1, p_2)^T \in \mathbb{R}^2\}$. Given a base point $q \in \mathbb{S}^1$, the exponential map $\exp_q : \mathbb{R} \rightarrow \mathbb{S}^1$ from the tangent space $T_q\mathbb{S}^1 \simeq \mathbb{R}$ of \mathbb{S}^1 at q onto \mathbb{S}^1 is 2π -periodic, i.e., $\exp_q(x) = \exp_q((x)_{2\pi})$ for any $x \in \mathbb{R}$, where $(x)_{2\pi}$ denotes the unique point in $[-\pi, \pi)$ such that $x = 2\pi k + (x)_{2\pi}$, $k \in \mathbb{Z}$. To guarantee the injectivity of the exponential map, we restrict its domain of definition from \mathbb{R} to $[-\pi, \pi)$. Thus, for $p, q \in \mathbb{S}^1$, there is now a unique $x \in [-\pi, \pi)$ satisfying $\exp_q(x) = p$. Given such representation system $x_j \in [-\pi, \pi)$ of $p_j \in \mathbb{S}^1$, $j = 1, 2$ centered at an arbitrary point q on \mathbb{S}^1 the geodesic distance becomes

$$d_{\mathbb{S}^1}(p_1, p_2) = d(x_1, x_2) = \min_{k \in \mathbb{Z}} |x_2 - x_1 + 2\pi k| = |(x_2 - x_1)_{2\pi}|. \quad (10)$$

Then, for $f, u : \mathcal{G} \rightarrow \mathbb{S}^1$, the cyclic equivalent of the discretized **data term** in (2) becomes

$$\mathcal{D}(u; f) := \frac{1}{2} \sum_{i,j=1}^{m,n} d(u_{i,j}, f_{i,j})^2.$$

To define a **regularization term** related to those in i) in Section 4 we need appropriate definitions of first and second order difference operators for cyclic data. For $w = (w_j)_{j=1}^\kappa \in \mathbb{R}^\kappa \setminus \{0\}$ with $\sum_{j=1}^\kappa w_j = 0$ a real-valued finite difference operator is given by $x \mapsto \langle x, w \rangle$. For cyclic data we consider similarly

$$d(x; w) := \min_{\alpha \in \mathbb{R}} \langle [x + \alpha 1_\kappa]_{2\pi}, w \rangle, \quad (11)$$

where 1_κ is the vector with κ entries 1 and $[x]_{2\pi}$ denotes the component-by-component application of $(t)_{2\pi}$ if $t \neq (2k+1)\pi$, $k \in \mathbb{Z}$ and $[(2k+1)\pi]_{2\pi} = \pm\pi$, $k \in \mathbb{Z}$. For $w_1 := (-1, 1)^\top$ definition (11) coincides with the geodesic distance, i.e., $d(x; w_1) = d(x_1, x_2)$ for all $x \in [-\pi, \pi]^2$. For the difference masks $w_2 := (1, -2, 1)^\top$ and $w_{1,1} := (-1, 1, 1, -1)^\top$ it can be shown [10] that

$$d(x; w_\nu) = |(\langle x, w_\nu \rangle)_{2\pi}|, \quad \nu \in \{2, (1, 1)\}.$$

It is remarkable that this relation does not hold true for other differences, e.g., for the third order difference $w = (-1, 3, -3, 1)^\top$. Introducing the notation

$$d_2(x) := d(x; w_2) \quad \text{and} \quad d_{1,1}(x) := d(x; w_{1,1})$$

the regularization term becomes

$$\mathcal{R}(u) := \text{TV}_1(u) + \text{TV}_2^{\text{hv}}(u) + \text{TV}_2^{\text{d}}(u) \quad (12)$$

with

$$\begin{aligned} \text{TV}_1(u) &:= \alpha_1 \sum_{i,j=1}^{n-1,m} d(u_{i,j}, u_{i+1,j}) + \alpha_2 \sum_{i,j=1}^{n,m-1} d(u_{i,j}, u_{i,j+1}), \\ \text{TV}_2^{\text{hv}}(u) &:= \beta_1 \sum_{i=1,j=2}^{n-1,m} d_2(u_{i-1,j}, u_{i,j}, u_{i+1,j}) + \beta_2 \sum_{i=2,j=1}^{n,m-1} d_2(u_{i,j-1}, u_{i,j}, u_{i,j+1}), \\ \text{TV}_2^{\text{d}}(u) &:= \beta_3 \sum_{i,j=1}^{n-1,m-1} d_{1,1}(u_{i,j}, u_{i+1,j}, u_{i,j+1}, u_{i+1,j+1}). \end{aligned}$$

Note that this regularizer corresponds to the so-called "anisotropic counterpart" of the regularization term in i) in Sections 3 and 4, i.e., roughly speaking it is related to

$$\int_{\Omega} \alpha_1 |\partial_{x_1} u| + \alpha_2 |\partial_{x_2} u| + \beta_1 |\partial_{x_1 x_1} u| + \beta_1 |\partial_{x_2 x_2} u| + \beta_3 |\partial_{x_1 x_2} u| dx.$$

6.3 Algorithm

As in the previous section we will apply an iterative algorithm which is based on analytic computations of proximal mappings of the difference functions $d(\cdot; w)$ similar to (9).

Proximal mapping of differences of cyclic data. As a cyclic counterpart to (9) we deal with

$$\begin{aligned} \text{prox}_{\lambda d(\cdot; w)}(f) &:= \arg \min_{x \in [-\pi, \pi]^\kappa} \mathcal{E}(x; g, w), \\ \mathcal{E}(x; g, w) &:= \frac{1}{2} \sum_{j=1}^{\kappa} d(x_j, f_j)^2 + \lambda d(x; w)^p, \quad \lambda > 0 \end{aligned}$$

for $w \in \{w_1, w_2, w_{1,1}\}$. Here $\arg \min_{x \in [-\pi, \pi]^\kappa}$ means that we are looking for the representative of $x \in (\mathbb{S}^1)^\kappa$ in $[-\pi, \pi]^\kappa$.

Theorem 6.1. [10] *For $w \in \{w_1, w_2, w_{1,1}\}$ set $s := \text{sgn}(\langle f, w \rangle)_{2\pi}$. Let $g \in [-\pi, \pi]^\kappa$, where κ is adapted to the respective length of w .*

1. *If $|(\langle g, w \rangle)_{2\pi}| < \pi$, then the unique minimizer of $\mathcal{E}(x; g, w)$ is given by*

$$\hat{x} = (g - s m w)_{2\pi}, \quad m := \min \left\{ \lambda, \frac{|(\langle g, w \rangle)_{2\pi}|}{\|w\|_2^2} \right\}.$$

2. *If $|(\langle g, w \rangle)_{2\pi}| = \pi$, then $\mathcal{E}(x; g, w)$ has the two minimizers*

$$\hat{x} = (g \mp s m w)_{2\pi}, \quad m := \min \left\{ \lambda, \frac{\pi}{\|w\|_2^2} \right\}.$$

Our proof in [10] uses the fact that

$$\begin{aligned} \mathcal{E}(x; f, w) &= \frac{1}{2} \sum_{j=1}^{\kappa} \min_{k_j \in \mathbb{Z}} |g_j - x_j - 2\pi k_j|^2 + \lambda \min_{\sigma \in \mathbb{Z}} |\langle x, w \rangle - 2\pi\sigma| \\ &= \min_{\substack{k \in \mathbb{Z}^\kappa \\ \sigma \in \mathbb{Z}}} \frac{1}{2} \|g - x - 2\pi k\|_2^2 + \lambda |\langle x, w \rangle - 2\pi\sigma|, \end{aligned}$$

so that the minimization can finally be restricted to those of real-valued data.

Cyclic proximal point algorithm (CPPA). Having an analytic expression for the proximal mappings of the cyclic finite differences at hand, our algorithm of choice to minimize the whole functional

$$J(u) := \mathcal{D}(u; f) + \mathcal{R}(u)$$

with $\mathcal{D}(u; f)$ in (10) and $\mathcal{R}(u)$ in (12) will be the cyclic proximal point algorithm (CPPA). The basic idea of the CPPA consists again in splitting the functional in an appropriate way as a sum $J = \sum_{l=1}^L J_l$ and to compute successively the proximal mappings of the summands J_l .

The proximal point algorithm (PP) on the Euclidean space goes back to [78] and was extended to Riemannian manifolds of non-positive sectional curvature in [46] and to Hadamard spaces in [5]. Its real-valued version computes $\arg \min_x g(x)$ for a proper, closed convex function g on \mathbb{R}^N by iterating

$$x^{(r)} := \text{prox}_{\lambda g}(x^{(r-1)}) = \arg \min_x \frac{1}{2} \|x^{(r-1)} - x\|_2^2 + \lambda g(x).$$

Finding $\arg \min_x g_1(x) + g_2(x)$ for the sum of two proper, closed convex function g_i , $i = 1, 2$ could be at the first glance performed similarly

$$x^{(r)} := \text{prox}_{\lambda g_2}(\text{prox}_{\lambda g_1}(x^{(r-1)})).$$

Since the concatenation of the two firmly non-expansive proximal operators is again firmly non-expansive the sequence of iterates $\{x^{(r)}\}_r$ converges, but unfortunately not to a minimizer of $g_1 + g_2$ but instead to the minimizer of ${}^\lambda g_1 + g_2$, where ${}^\lambda g_1$ denotes the Moreau envelope of g_1 . Convergence to the minimizer of the desired sum $g_1 + g_2$ can be achieved by varying the parameter λ within the iterations. More precisely, the CPPA computes $\arg \min_x \sum_{l=1}^L g_l(x)$ by

$$x^{(k)} = \text{prox}_{\lambda_k g_L} \left(\text{prox}_{\lambda_k g_{L-1}} \left(\dots \text{prox}_{\lambda_k g_1} (x^{(k-1)}) \right) \right),$$

where

$$\sum_{k=0}^{\infty} \lambda_k = \infty, \quad \text{and} \quad \sum_{k=0}^{\infty} \lambda_k^2 < \infty. \quad (13)$$

This CPPA on the Euclidean space was given in [16], see also the survey [15]. A CPPA for Hadamard spaces can be found in [6]. With first order differences of cyclic data in the regularization term the CPPA was applied for image restoration in [101].

For our functional J we use a splitting into $L = 6$ (in one dimension) and $L = 15$ (in two dimensions) summands which correspond to the natural splitting of the image grid into disjoint parts by the difference operators. For example we apply for the first summand in TV_2^{hv} the splitting into the three parts

$$\sum_{\nu=0}^2 \sum_{i=1}^{\lfloor \frac{n-1}{3} \rfloor} \sum_{j=1}^m d_2(u_{3i-2+\nu,j}, u_{3i-1+\nu,j}, u_{3i+\nu,j}).$$

Convergence. Since \mathbb{S}^1 is not a Hadamard space, the convergence analysis of the CPPA in [6] cannot be applied. However, convergence can be proved under certain conditions: i) the data $f \in (\mathbb{S}^1)^{n,m}$ is locally dense enough, which means that the distance between neighboring pixel values

$$d_\infty(f) := \max_{(i,j) \in \mathbb{I}} \max_{(k,l) \in N_{i,j}} d(f_{i,j}, f_{k,l}), \quad N_{i,j} := \{(k,l) \in \mathbb{I} : |i-k| + |l-j| = 1\}$$

is sufficiently small. ii) The regularization parameters α, β are sufficiently small. More precisely, we assume that for some $\varepsilon > 0$ we have

$$\text{TV}_1(f) + \text{TV}_2^{\text{hv}}(f) + \text{TV}_2^{\text{d}}(f) \leq \frac{\varepsilon^2}{\mu}, \quad (14)$$

where $\mu := \max\{\alpha_1, \alpha_2, \beta_1, \beta_2, \beta_3\} > 0$. iii) Condition (13) must be fulfilled.

Theorem 6.2. [10] *Let $f \in (\mathbb{S}^1)^{n,m}$ with $d_\infty(f) < \frac{\pi}{8}$. Let $\lambda := \{\lambda_k\}_k$ fulfill property (13) and*

$$\sqrt{\varepsilon^2 + 32\|\alpha\|_2^2 L(L+1) + 8\|\alpha\|_\infty L} < \frac{\pi}{16},$$

for some $\varepsilon > 0$, where $L = 15$. Further, assume that the parameters α, β of the functional J and ε satisfy (14). Then the sequence $\{u^{(k)}\}_k$ generated by the CPPA converges to a global minimizer of J .

6.4 Numerical Results

In this section we demonstrate the performance of our algorithms by numerical examples with artificial signals and images. For real-world applications in synthetic aperture radar and for the analysis of electroencephalograms we refer to [10].

We start by demonstrating the influence of first and/or second order differences on the denoising process for one-dimensional data.

The function $g : [0, 1] \rightarrow [-\pi, \pi]$ given by

$$g(x) := \begin{cases} -24\pi x^2 + \frac{3}{4}\pi & \text{for } 0 \leq x \leq \frac{1}{4}, \\ 4\pi x - \frac{\pi}{4} & \text{for } \frac{1}{4} < x \leq \frac{3}{8}, \\ (-\pi x - \frac{3}{8})_{2\pi} & \text{for } \frac{3}{8} < x \leq \frac{1}{2}, \\ (-\frac{j+7}{8}\pi)_{2\pi} & \text{for } \frac{3j+16}{32} < x \leq \frac{3j+19}{32}, j = 0, 1, 2, 3, \\ \frac{3}{2}\pi \exp(-\frac{35}{7} - \frac{1}{1-x}) - \frac{3}{4}\pi & \text{for } \frac{7}{8} < x \leq 1, \end{cases}$$

was sampled equidistantly to obtain the original signal u_0 at $N = 500$ samples. This function is distorted by wrapped Gaussian noise η of standard deviation $\sigma = \frac{1}{5}$ to get f in Fig. 9 (a). Note that the linear increase on $[\frac{1}{4}, \frac{3}{8}]$

of g is continuous and the change from π to $-\pi$ at $\frac{5}{16}$ is just due to the chosen representation system in $[-\pi, \pi)$. Similarly the two constant parts with the values $-\pi$ and $\frac{7}{8}\pi$ differ only by a jump size of $-\frac{\pi}{8}$. In the representation system $[0, 2\pi)$ the signal looks as in Fig. 9 (b). We apply our method with different model parameters α and β to f which yields the restored signals u_r . The parameters were optimized with respect to the restoration error measured by the ‘cyclic’ mean squared error

$$e(u_0, u_r) := \frac{1}{N} \sum_{i=1}^M d(u_{0,i}, u_{r,i})^2.$$

The resulting signal u_r is depicted in Fig. 9 (c)-(e). Fig. 9 (f) shows the result from Fig. 9 (e) with respect to another representation system.

Next we consider the synthetic surface given on $[0, 1]^2$ shown in Fig. 10 (a). This surface consists of two plates of height $\pm 2\pi$ divided at the diagonal, a set of stairs in the upper left corner in direction $\frac{\pi}{3}$, a linear increasing area connecting both plateaus having the shape of an ellipse with major axis at the angle $\frac{\pi}{6}$, and a half ellipsoid forming a dent in the lower right of the image with circular diameter of size $\frac{9}{25}$ and depth 4π . The initial data is given by sampling the described surface at $m = n = 256$ sampling points. Then Gaussian noise is added and the data is wrapped, see 10 (b) and (c). Fig. 10 (d)-(f) show the denoising results with different regularization terms. The parameters were chosen from $\frac{1}{8}\mathbb{N}$ such that they minimize the cyclic mean squared error.

Finally, Fig. 11 shows an artificial inpainting example with cyclic second order regularization terms. The original image u_0 is corrupted by a non-invertible masking operator K which gives f . Here no noise is added. The masking operator K has to be involved into the data term of the functional. For the precise description of the setting we refer to [11]. The results were further extended to $\mathbb{S}^1 \times \mathbb{R}^d$ -valued data in [12].

Acknowledgement: Funding by the Deutsche Forschungsgemeinschaft (DFG) within the RTG GrK 1932 ”Stochastic Models for Innovations in the Engineering Sciences”, project area P3, and within the DFG Grant STE571/11-1 is gratefully acknowledged.

References

- [1] L. Alvarez, C. Castaño, M. García, K. Krissian, L. Mazorra, A. Salgado, and J. Sánchez. Variational second order flow estimation for PIV sequences. *Experiments in Fluids*, 44(2):291–304, 2008.
- [2] L. Ambrosio, N. Fusco, and D. Pallara. *Functions of Bounded Variation and Free Discontinuity Problems*. Oxford University Press, Oxford, 2000.

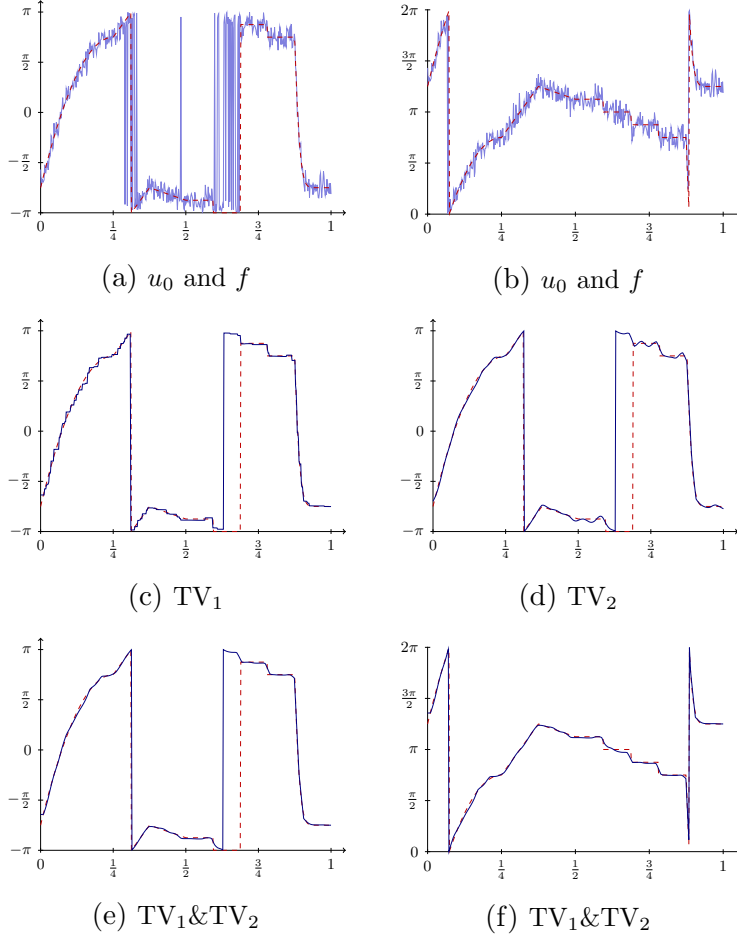


Figure 9. Denoising of a one-dimensional signal with CPPA. (a) Original signal u_0 (dashed red) and disturbed signal by wrapped Gaussian noise f (solid black). (b) shows the signals from (a) with respect to $[0, 2\pi)$. (c)—(e) Reconstructed signals u_r using (c) only the TV_1 regularizer, $e(u_0, u_r) \approx 6.06 \times 10^{-3}$, (d) only the TV_2 regularizer, $e(u_0, u_r) \approx 4.34 \times 10^{-3}$, and (e) both of them, $e(u_0, u_r) \approx 3.53 \times 10^{-3}$. While (c) suffers from the staircasing effect, (d) shows weak results at constant areas. The combination of both regularizers in (e) yields the best image. (f) shows signal (e) in $[0, 2\pi)$.

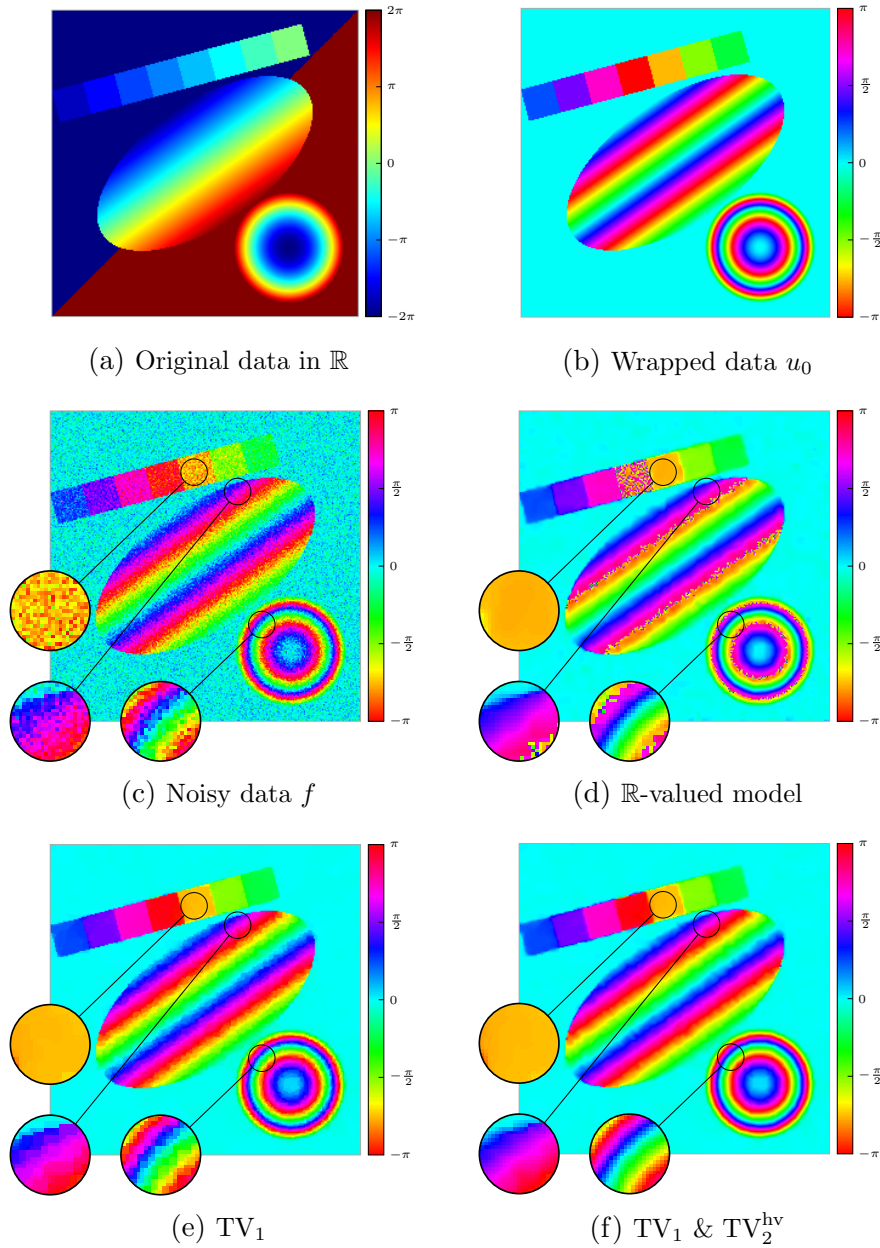


Figure 10. Denoising of an artificial surface: (c) wrapped image (b) of (a) corrupted by wrapped Gaussian noise. Reconstructed images u_r using (d) the real-valued first plus second order regularization i). The results at near $\pm\pi$ are poor. (e) the cyclic TV_1 regularizer, $e(u_0, u_r) = 7.09 \times 10^{-3}$. Here u_r reproduces the piecewise constant parts of the stairs in the upper left part and the background, but introduces a staircasing in both linear increasing areas inside the ellipse and in the half ellipsoid. (f) the regularizer in (12), $e(u_0, u_r) = 5.37 \times 10^{-3}$. Combining first and second order cyclic differences improves the results.

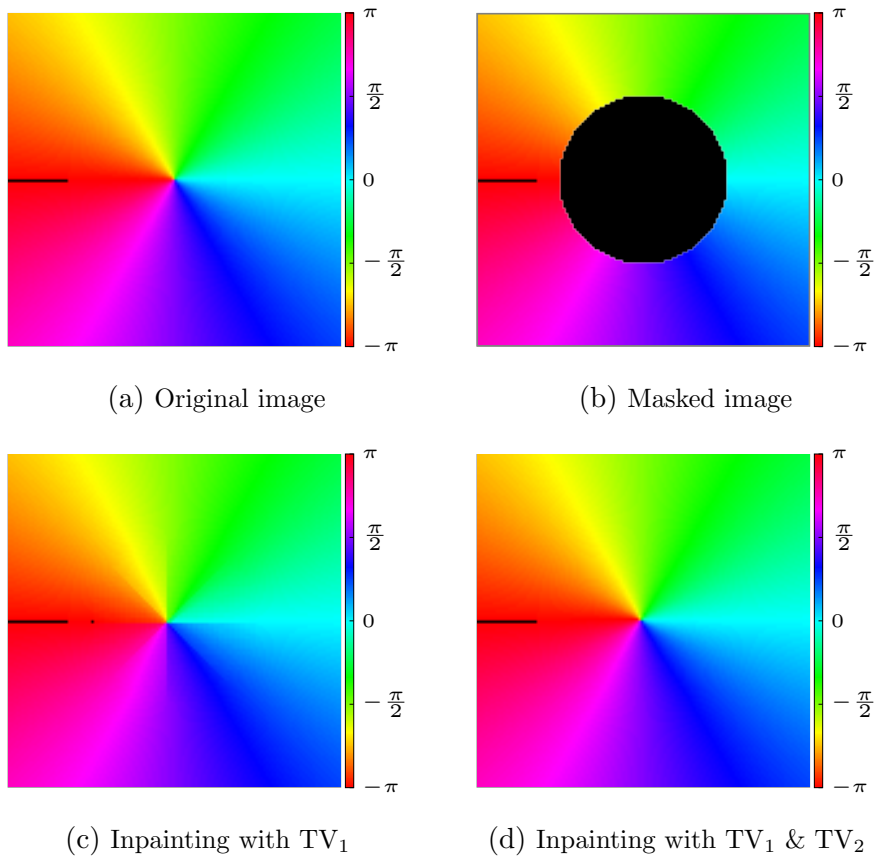


Figure 11. Original image (a) and its masked version (b). The first reconstruction (c) employs only first order cyclic differences and produces staircasing. Combining first and second order cyclic differences in (d) we obtain a nearly perfect reconstruction. (Image source: Courtesy of R. Bergmann, [11]).

- [3] P. Anandan. A computational framework and an algorithm for the measurement of visual motion. *International Journal of Computer Vision*, 2(3):283–310, 1989.
- [4] S. Babacan, R. Molina, and A. Katsaggelos. Parameter estimation in TV image restoration using variational distribution approximation. *IEEE Transactions on Image Processing*, 17(3):326–339, 2008.
- [5] M. Bačák. The proximal point algorithm in metric spaces. *Israel Journal of Mathematics*, 194(2):689–701, 2013.
- [6] M. Bačák. Computing medians and means in Hadamard spaces. *to appear in SIAM Journal of Optimization*, 2014.
- [7] F. Balle, D. Eifler, J. H. Fitschen, S. Schuff, and G. Steidl. Computation and visualization of local deformation for multiphase metallic materials by infimal convolution of TV-type functionals. *ArXiv Preprint*, 2014.
- [8] J. M. Bardsley. Wavefront reconstruction methods for adaptive optics systems on ground-based telescopes. *SIAM Journal Matrix Analysis and Applications*, (30):67–83, 2008.
- [9] F. Becker, S. Petra, and C. Schnörr. Optical flow. In O. Scherzer, editor, *Handbook of Mathematical Methods in Imaging*. Springer, 2nd edition, 2014.
- [10] R. Bergmann, F. Laus, G. Steidl, and A. Weinmann. Second order differences of cyclic data and applications in variational denoising. *SIAM Journal on Imaging Sciences*, 7(4):2916–2953, 2014.
- [11] R. Bergmann and A. Weinmann. Inpainting of cyclic data using first and second order differences. In *EMCVPR2015*, Lecture Notes in Computer Science, pages 155–168, 2015.
- [12] R. Bergmann and A. Weinmann. A second order TV-type approach for inpainting and denoising higher dimensional combined cyclic and vector space data. *ArXiv Preprint*, 1501.02684, 2015.
- [13] M. Bergounioux and L. Piffet. A second-order model for image denoising. *Set-Valued and Variational Analysis*, 18(3-4):277–306, 2010.
- [14] M. Bertero and P. Boccacci. *Introduction to Inverse Problems in Imaging*. IoP Publishing, Bristol, 1998.
- [15] D. P. Bertsekas. Incremental gradient, subgradient, and proximal methods for convex optimization: a survey. Technical Report LIDS-P-2848, Laboratory for Information and Decision Systems, MIT, Cambridge, MA, 2010.

- [16] D. P. Bertsekas. Incremental proximal methods for large scale convex optimization. *Mathematical Programming, Series B*, 129(2):163–195, 2011.
- [17] J. Bioucas-Dias, V. Katkovnik, J. Astola, and K. Egiazarian. Absolute phase estimation: adaptive local denoising and global unwrapping. *Applied Optics*, 47(29):5358–5369, 2008.
- [18] J. Bioucas-Dias and G. Valadão. Phase unwrapping via graph cuts. *IEEE Transactions on Image Processing*, 16(3):698–709, 2007.
- [19] J. Blaber, B. Adair, and A. Antoniou. Ncorr: Open-source 2D digital image correlation Matlab software. <http://www.ncorr.com>, 2014.
- [20] R. I. Boş and C. Hendrich. Convergence analysis for a primal-dual monotone + skew splitting algorithm with applications to total variation minimization. *Journal of Mathematical Imaging and Vision*, 49(3):551–568, 2014.
- [21] K. Bredies, K. Kunisch, and T. Pock. Total generalized variation. *SIAM Journal on Imaging Sciences*, 3(3):1–42, 2010.
- [22] K. Bredies and T. Valkonen. Inverse problems with second-order total generalized variation constraints. In *Proceedings of SampTA 2011 2011 - 9th International Conference on Sampling Theory and Applications*, 2011.
- [23] T. Brox, A. Bruhn, N. Papenberg, and J. Weickert. High accuracy optical flow estimation based on a theory for warping. In T. Pajdla and J. Matas, editors, *Computer Vision - ECCV 2004*, volume 3024 of *Lecture Notes in Computer Science*, pages 25–36. Springer Berlin Heidelberg, 2004.
- [24] T. Brox and J. Malik. Large Displacement Optical Flow: Descriptor Matching in Variational Motion Estimation. *IEEE Transactions on Pattern Analysis and Machine Intelligence*, 33(3):500–513, 2011.
- [25] M. Burger, A. Sawatzky, and G. Steidl. First order algorithms in variational image processing. *ArXiv Preprint*, 1412.4237, 2014.
- [26] J.-F. Cai, R. Chan, and M. Nikolova. Fast two-phase image deblurring under impulse noise. *Journal of Mathematical Imaging and Vision*, 36(1):46–53, 2010.
- [27] A. Chambolle, V. Caselles, D. Cremers, M. Novaga, and T. Pock. An introduction to total variation for image analysis. *Theoretical Foundations and Numerical Methods for Sparse Recovery*, 9:263–340, 2010.

- [28] A. Chambolle and P.-L. Lions. Image recovery via total variation minimization and related problems. *Numerical Mathematics*, 76(2):167–188, 1997.
- [29] A. Chambolle and T. Pock. A First-Order Primal-Dual Algorithm for Convex Problems with Applications to Imaging. *Journal of Mathematical Imaging and Vision*, 40(1):120–145, 2011.
- [30] R. H. Chan, X. Yuan, and W. Zhang. A phase model for point spread function estimation in ground-based astronomy. *Preprint Chinese University of Hongkong*, 2014.
- [31] T. F. Chan, S. Esedoglu, and F. E. Park. Image decomposition combining staircase reduction and texture extraction. *Journal of Visual Communication and Image Representation*, 18(6):464–486, 2007.
- [32] T. F. Chan, S. H. Kang, and J. Shen. Euler’s elastica and curvature-based inpainting. *SIAM Journal on Applied Mathematics*, pages 564–592, 2002.
- [33] T. F. Chan, A. Marquina, and P. Mulet. High-order total variation-based image restoration. *SIAM Journal on Scientific Computation*, 22(2):503–516, 2000.
- [34] Q. Chu, S. Jefferies, and J. G. Nagy. Iterative wavefront reconstruction for astronomical imaging. *SIAM Journal on Scientific Computing*, to appear.
- [35] P. Combettes and J.-C. Pesquet. Primal-dual splitting algorithm for solving inclusions with mixture of composite, Lipschitzian, and parallel-sum type monotone operators. *Set-Valued and Variational Analysis*, 20(2):307–330, 2012.
- [36] P. L. Combettes and J.-C. Pesquet. Proximal splitting methods in signal processing. In *Fixed-Point Algorithms for Inverse Problems in Science and Engineering*, pages 185–212. Springer, 2011.
- [37] P. L. Combettes and V. R. Wajs. Signal recovery by proximal forward-backward splitting. *Multiscale Modeling and Simulation*, 4:1168–1200, 2005.
- [38] D. Cremers and S. Soatto. Motion competition: A variational approach to piecewise parametric motion segmentation. *International Journal of Computer Vision*, 62(3):249–265, 2005.
- [39] C.-A. Deledalle, L. Denis, and F. Tupin. NL-InSAR: Nonlocal interferogram estimation. *IEEE Transactions on Geoscience Remote Sensing*, 49(4):1441–1452, 2011.

- [40] F. Demengel. Fonctions á Hessian borne: *Annals of Institute Fourier*, 34:155–190, 1985.
- [41] S. Didas, G. Steidl, and S. Setzer. Combined ℓ_2 data and gradient fitting in conjunction with ℓ_1 regularization. *Advances in Computational Mathematics*, 30(1):79–99, 2009.
- [42] S. Didas, J. Weickert, and B. Burgeth. Properties of higher order nonlinear diffusion filtering. *Journal of Mathematical Imaging and Vision*, 35:208–226, 2009.
- [43] J. Douglas and H. H. Rachford. On the numerical solution of heat conduction problems in two and three space variables. *Transactions of the American Mathematical Society*, 82(2):421–439, 1956.
- [44] H. W. Engl, M. Hanke, and A. Neubauer. *Regularization of Inverse Problems*. Kluwer, Dordrecht, 1996.
- [45] E. Esser, X. Zhang, and T. F. Chan. A general framework for a class of first order primal-dual algorithms for convex optimization in imaging science. *SIAM Journal Imaging Sciences*, 3(4):1015–1046, 2010.
- [46] O. P. Ferreira and P. R. Oliveira. Proximal point algorithm on Riemannian manifolds. *Optimization*, 51(2):257–270, 2002.
- [47] N. I. Fisher. *Statistical Analysis of Circular Data*. Cambridge University Press, 1995.
- [48] S. Foucart and H. Rauhut. *A Mathematical Introduction to Compressive Sensing*. Birkhäuser, 2013.
- [49] M. Giaquinta, G. Modica, and J. Souček. Variational problems for maps of bounded variation with values in S^1 . *Calculus of Variation*, 1(1):87–121, 1993.
- [50] M. Giaquinta and D. Mucci. The BV-energy of maps into a manifold: relaxation and density results. *Annali della Scuola Normale - Classe di Scienze*, 5(4):483–548, 2006.
- [51] M. Giaquinta and D. Mucci. Maps of bounded variation with values into a manifold: total variation and relaxed energy. *Pure Applied Mathematics Quarterly*, 3(2):513–538, 2007.
- [52] B. Goldluecke, E. Strelakovski, and D. Cremers. A natural total variation which arises from geometric measure theory. *SIAM Journal on Imaging Sciences*, 5(2):537–563, 2012.

- [53] D. Goldstein and S. Osher. The Split Bregman method for l_1 regularized problems. *SIAM Journal on Imaging Sciences*, 2(2):323–343, 2009.
- [54] T. Goldstein, E. Esser, and R. Baraniuk. Adaptive primal-dual hybrid gradient methods for saddle-point problems. *Preprint, arXiv*, 2013.
- [55] J. W. Goodman. *Introduction to Fourier Optics*. McGraw-Hill, 1996.
- [56] Y. Gousseau and J.-M. Morel. Are natural images of bounded variation? *SIAM Journal on Mathematical Analysis*, 33(3):634–648, 2001.
- [57] F. Greb, T. Krivobokova, A. Munck, and S. von Cramon-Taubadel. Regularized bayesian estimation in generalized threshold regression methods. *Bayesian Analysis*, 9(1):171–196, 2014.
- [58] M. Hanke and P. C. Hansen. Regularization methods for large-scale problems. *Survey on Mathematics for Industry*, 3:253–315, 1993.
- [59] A. Hoyer, J. Weickert, H. Seibert, T. Scheffer, and S. Diebels. Lagrangian strain tensor computation with higher order variational models. In *Proceedings of the British Machine Vision Conference*. BMVA Press, 2013.
- [60] W. Hinterberger and O. Scherzer. Variational methods on the space of functions of bounded Hessian for convexification and denoising. *Computing*, 76(1):109–133, 2006.
- [61] W. Hinterberger, O. Scherzer, C. Schnörr, and J. Weickert. Analysis of optical flow models in the framework of calculus of variations. *SIAM Journal on Applied Mathematics*, 23(1/2):69–89, 2002.
- [62] W. Hintermüller and K. Kunisch. Total bounded variation regularization as a bilaterally constrained optimization problem. *SIAM Journal on Applied Mathematics*, 64(4):1311–1333, May 2004.
- [63] M. Holler and K. Kunisch. On infimal convolution of tv type functionals and applications to video and image reconstruction. *SIAM Journal on Imaging Sciences*, 7(4):2258–2300, 2014.
- [64] B. K. Horn and B. G. Schunck. Determining optical flow. *Artificial Intelligence*, 17(1-3):185–203, 1981.
- [65] J. M. Hyman and M. J. Shashkov. Natural discretizations for the divergence, gradient, and curl on logically rectangular grids. *Computational and Mathematical Applications*, 33(4):81–104, 1997.

- [66] K. V. Ivanov, V. V. Vasin, and V. P. Tanana. *Theory of Linear Ill-Posed Problems and its Applications*. Brill Academic Publishers, Utrecht, Boston, Koeln, Tokyo, 2002.
- [67] S. R. Jammalamadaka and A. SenGupta. *Topics in Circular Statistics*. World Scientific Publishing Company, 2001.
- [68] C. L. Lawson and R. J. Hansen. *Solving least squares problems*. Prentice-Hall, Englewood Cliffs, 1974.
- [69] S. Lefkimmiatis, A. Bourquard, and M. Unser. Hessian-based norm regularization for image restoration with biomedical applications. *IEEE Transactions on Image Processing*, 21(3):983–995, 2012.
- [70] J. Lellmann, E. Strelakovsky, S. Koetter, and D. Cremers. Total variation regularization for functions with values in a manifold. In *IEEE ICCV 2013*, pages 2944–2951, 2013.
- [71] P. L. Lions and B. Mercier. Splitting algorithms for the sum of two nonlinear operators. *SIAM Journal on Numerical Analysis*, 16(6):964–979, 1979.
- [72] M. Lysaker, A. Lundervold, and X.-C. Tai. Noise removal using fourth-order partial differential equations with applications to medical magnetic resonance images in space and time. *IEEE Transactions on Image Processing*, 12(12):1579–1590, 2003.
- [73] S. Mallat. *A Wavelet Tour of Signal Processing*. Academic Press, 1999.
- [74] G. D. Maso, I. Fonseca, G. Leoni, and M. Morini. A higher order model for image restoration: The one-dimensional case. *SIAM Journal on Mathematical Analysis*, 40(6):2351–2391, 2009.
- [75] V. A. Morozov. *Methods for Solving Incorrectly Posed Problems*. Springer, New York, 1984.
- [76] K. Papafitsoros and C. B. Schönlieb. A combined first and second order variational approach for image reconstruction. *Journal of Mathematical Imaging and Vision*, 2(48):308–338, 2014.
- [77] T. Pock, A. Chambolle, D. Cremers, and H. Bischof. A convex relaxation approach for computing minimal partitions. In *IEEE Conf. Computer Vision and Pattern Recognition*, pages 810–817. 2009.
- [78] R. T. Rockafellar. Monotone operators and the proximal point algorithm. *SIAM Journal on Control and Optimization.*, 14(5):877–898, 1976.

- [79] L. I. Rudin, S. Osher, and E. Fatemi. Nonlinear total variation based noise removal algorithms. *Physica D*, 60(1):259–268, 1992.
- [80] B. W. Rust and D. P. O’Leary. Residual periodograms for choosing regularization parameters for ill-posed problems. *Inverse Problems*, 24(3):034005, 2008.
- [81] G. Sapiro. Vector-valued active contours. *IEEE CVPR 1996*, pages 680–685.
- [82] A. Sawatzky, C. Brune, T. Kösters, F. Wübbeling, and M. Burger. EM-TV methods for inverse problems with Poisson noise. In *Level Set and PDE Based Reconstruction Methods in Imaging*, pages 71–142, 2013.
- [83] S. Scherer, P. Werth, and A. Pinz. The discriminatory power of ordinal measures - towards a new coefficient. In *Computer Vision and Pattern Recognition, 1999. IEEE Computer Society Conference on.*, volume 1, pages 76–81, 1999.
- [84] O. Scherzer. Denoising with higher order derivatives of bounded variation and an application to parameter estimation. *Computing*, 60(1):1–27, 1998.
- [85] O. Scherzer, M. Grasmair, H. Grossauer, M. Haltmeier, and F. Lenzen. *Variational methods in imaging*. Springer, 2009.
- [86] S. Setzer. Operator splittings, Bregman methods and frame shrinkage in image processing. *International Journal of Computer Vision*, 92(3):265–280, 2011.
- [87] S. Setzer and G. Steidl. Variational methods with higher order derivatives in image processing. In *Approximation XII: San Antonio 2007*, pages 360–385, 2008.
- [88] S. Setzer, G. Steidl, and T. Teuber. Infimal convolution regularizations with discrete l1-type functionals. *Communications in Mathematical Sciences*, 9(3):797–872, 2011.
- [89] G. Steidl and T. Teuber. Removing multiplicative noise by Douglas-Rachford splitting methods. *Journal of Mathematical Imaging and Vision*, 36(2):168–184, 2010.
- [90] D. J. Strauss, T. Teuber, G. Steidl, and F. I. Corona-Strauss. Exploiting the self-similarity in ERP images by nonlocal means for single-trial denoising. *IEEE Transactions on Neural System and Rehabilitation Engineering*, 21(4):576–583, 2013.

- [91] E. Strekalovskiy and D. Cremers. Total variation for cyclic structures: Convex relaxation and efficient minimization. In *IEEE CVPR 2011*, pages 1905–1911. IEEE, 2011.
- [92] E. Strekalovskiy and D. Cremers. Total cyclic variation and generalizations. *Journal of Mathematical Imaging and Vision*, 47(3):258–277, 2013.
- [93] X.-C. Tai, J. Hahn, and G. J. Chung. A fast algorithm for euler’s elastica model using augmented lagrangian method. *SIAM Journal on Imaging Sciences*, 4(1):313–344, 2011.
- [94] A. Tatzschl and O. Kolednik. A new tool for the experimental characterization of micro-plasticity. *Materials Science and Engineering: A*, 339(1–2):265 – 280, 2003.
- [95] T. Teuber, G. Steidl, and R. H. Chan. Minimization and parameter estimation for seminorm regularization models with I-divergence constraints. *Inverse Problems*, 29:1–28, 2013.
- [96] W. Trobin, T. Pock, D. Cremers, and H. Bischof. An unbiased second-order prior for high-accuracy motion estimation. In G. Rigoll, editor, *Pattern Recognition*, volume 5096 of *Lecture Notes in Computer Science*, pages 396–405. Springer Berlin Heidelberg, 2008.
- [97] B. C. Vũ. A splitting algorithm for dual monotone inclusions involving cocoercive operators. *Advances in Computational Mathematics*, 38(3):667–681, 2013.
- [98] G. Wahba. Practical approximate solutions to linear operator equations when the data are noisy. *SIAM Journal on Numerical Analysis*, 14(4):651–667, 1977.
- [99] J. Weickert and C. Schnörr. Variational optic flow computation with a spatio-temporal smoothness constraint. *Journal of Mathematical Imaging and Vision*, 14(3):245–255, May 2001.
- [100] J. Weickert, M. Welk, and M. Wickert. L2-stable nonstandard finite differences for anisotropic diffusion. In *Scale-Space and Variational Methods in Computer Vision 2013*, volume 7893 of *Lecture Notes in Computer Science*, pages 380–391, 2013.
- [101] A. Weinmann, L. Demaret, and M. Storath. Total variation regularization for manifold-valued data. *SIAM Journal on Imaging Sciences*, 7(4):2226–2257, 2014.
- [102] M. Welk, G. Steidl, and J. Weickert. Locally analytic schemes: A link between diffusion filtering and wavelet shrinkage. *Applied and Computational Harmonic Analysis*, 24:195–224, 2008.

- [103] J. Yuan, C. Schnörr, and E. Mémin. Discrete orthogonal decomposition and variational fluid flow estimation. *Journal of Mathematical Imaging and Vision*, (28):67–80, 2007.
- [104] J. Yuan, C. Schnörr, and G. Steidl. Simultaneous higher order optical flow estimation and decomposition. *SIAM Journal on Scientific Computing*, 29(6):2283–2304, 2007.
- [105] J. Yuan, C. Schnörr, and G. Steidl. Convex Hodge decomposition and regularization of image flows. *Journal of Mathematical Imaging and Vision*, 33(2):169–177, 2009.



CV: Gabriele Steidl received her PhD and Habilitation in Mathematics from the University of Rostock, Germany, in 1988 and 1991, respectively. From 1993 to 1996, she held a position as assistant professor of Applied Mathematics at the University of Darmstadt, Germany. From 1996 to 2010, she was full professor at the Department of Mathematics and Computer Science, University of Mannheim, Germany. Since 2011, she is Professor at the Department of Mathematics, University of Kaiserslautern, Germany. Her research interests include applied and computational harmonic analysis and convex analysis with applications in image processing.